12-1-2002

Design and Control of a Compliant Parallel Manipulator

Thomas G. Sugar
Arizona State University

R. Vijay Kumar
University of Pennsylvania, kumar@grasp.upenn.edu

DESIGN AND CONTROL OF A COMPLIANT PARALLEL MANIPULATOR

Thomas G. Sugar *

Mechanical and Aerospace Engineering
Arizona State University
Tempe, Arizona 85287
Email: thomas.sugar@asu.edu

Vijay Kumar

General Robotics and Active Sensory Perception
(GRASP) Laboratory
University of Pennsylvania
Philadelphia, Pennsylvania 19104

Abstract

We describe a novel design for a compliant arm that can be mounted on a mobile robot. Because the arm is compliant, a mobile robot can manipulate or interact with objects that are not precisely positioned in the environment. The main features of the arm are the in-parallel architecture and a novel control scheme that allows us to easily control the Cartesian stiffness or impedance in the plane. Springs are added in series to the limbs of the parallel manipulator. We analyze one limb and the manipulator to determine its performance when either controlling the force applied to an object or controlling its stiffness. Further, we present experimental results that show the performance of the compliant arm.

1 Background

Whitney (1985) gives a historical viewpoint on the state of robot force control and believes better controllers which account for the robot's compliance are needed in order to improve stability. Whitney describes many different types of robot controllers such as a hybrid position/force controller, an explicit force controller, an impedance controller, and an active compliance controller. All of these methods are used to control existing robots designed for position control tasks, not force control tasks. Controlling the force at the end of a robot is a challenging problem because of instabilities. Eppinger and Seering (1986) describe the instability as sustained oscillations when a robot contacts the environment. They give a qualitative analysis showing the instability is not only due to digital sampling, friction and backlash, but is also due to the higher order dynamics of the robot and the positioning of the sensor at a remote point from the robot. When a position control law is used to control the force, it is unstable because it attempts to regulate the force through a dynamic system, namely the robot itself. An in-depth discussion on impedance control is given by many authors such as Hogan and Kazerooni (Colgate and Hogan, 1988; Kazerooni et al., 1986a,b). Explicit force control algorithms are tested on an experimental system and an integral controller is shown to be superior (Volpe and Khosla, 1992). Mason (1981) describes a kinematic representation for the the space of force controlled directions and the space of position controlled directions which can then be used as inputs to a hybrid position/force controller.

---

* Address all correspondence to this author.

In designing a compliant arm for grasping tasks, a system is needed which can easily control the forces in the plane. The traditional approach is to actively control the compliance of the system using appropriate control algorithms developed by Paul and Shimano (1976); Salisbury (1980); Xu and Paul (1988). The main disadvantage is that in such systems, the mechanical stiffness is typically very large and it is necessary to rely on high-performance actuators and high bandwidth control to produce compliance with robots that are particularly designed for position control tasks. Such schemes have inherent limitations during interaction with stiff environments.

In contrast to this approach, it is possible to build into the system some mechanical compliance and then use active control to vary this compliance. The main advantage of this approach is that there is always some compliance in the system regardless of the stiffness of the environment. As a result, the requirements on the actuator and the control bandwidth are more modest.

Many researchers have built devices that allow the mechanical compliance to be varied. Sugano et al. (1992) designed a finger that incorporates a leaf spring that can be adjusted in order to vary the joint compliance. The joint was not mounted rigidly but could move according to the compliance of the leaf spring. De Uri Tasch designed a two degree-of-freedom finger which again uses leaf springs but it has the ability to control the coupling compliance as well (Tasch, 1996). A similar approach to ours is proposed in (Pratt and Williamson, 1995) where they describe a series elastic actuator for a humanoid robot. They use an impedance control scheme to control the compliance of a one degree-of-freedom rotary joint. Other researchers, Morrell and Salisbury (1995), have also tried to control the stiffness by using a large compliant actuator coupled with a stiff micro actuator. A variant of this idea is used in our previous work (Pfreundschuh et al., 1994) where we developed a compliant wrist to be mounted on a stiff robot arm. Recently, a new actuator employing biomimetic research was developed by Kolacinski and Quinn (1998) that can modulate the position and stiffness of the actuator although the system's stiffness law is very complicated. Instead of controlling the stiffness, Howell and others designed a unique constant force generating mechanism which relies on the antagonistic action of springs (Howell et al., 1994).

While the fundamental idea of adding mechanical compliance underlying our design is similar to the previously mentioned work, the actual design and implementation are very different and our design can be extended to six degree-of-freedom manipulators on mobile platforms by adding more limbs in parallel. In our design, a linear spring is added in series to the limb and the equilibrium position of the spring is controlled to exert a desired force. The compliance is actively changed using a control law instead of fixing the compliance by passively adding springs. Secondly, the force control problem is converted to a simple position control problem using simple electric motors. The system is inherently passive because the position controller only adjusts the tension or compression of the spring. Lastly, we can modulate both the home position and stiffness of the limb.

2 Arm Design

The arm design and kinematics are presented for a planar, parallel mechanism which is an integral part of a team of position controlled robots in order to control the grasp forces and accommodate the robots' position errors. Candidate arm designs are discussed and for completeness optimal designs of planar mechanisms are also presented.

2.1 Mobile Manipulator Design

Our design solution consists of a three degree-of-freedom parallel manipulator with springs actuated with inexpensive DC servo motors. The planar parallel manipulator shown in Figures 1, 3, and 4 allows forces to be applied in the X and Y direction as well as a moment in the Z direction. During the design stage, the complexity of the controller and the required computer and electronics are considered. In our method, the plant is altered to achieve the best possible mechanical design and control solution. Because the mobile platforms have a suitable electrical source, DC motors are considered along with a suitable control scheme for the DC motors. The design uses a simple motor and motor control scheme because accurate position control algorithms for DC motors already exist on embedded motor processors. With these added constraints on the mechanical design, a new, innovative design is conceived that reduces the complexity of the controller by optimizing both the control and mechanical parameters during the initial design stage.
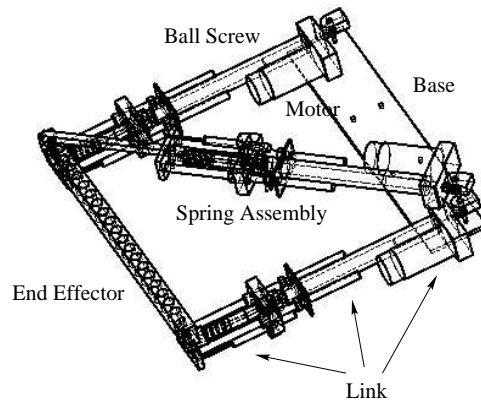
Figure 1.   The planar parallel manipulator.

Each limb of the parallel manipulator is a linear actuator with a spring system in series. The linear actuator is a DC servo motor with a ball screw transmission. The compression of the spring is measured by a high precision linear encoder (5000 counts per inch) and the actuator force is easily obtained by measuring the deflection. While the stiffness of the springs cannot be changed, the equilibrium position of a spring can be changed quickly by altering the actuator position. This has the effect of changing the effective stiffness of the limb. The forces of each limb are determined by the deflection of a linear spring in contrast to torque control of motors with large gear ratios, inertia, and backlash.

The parallel geometry allows for high stiffness (other than the springs), direct drive of the limbs, and mounting of the motors near the base. Because the direct kinematics is very complicated, redundant encoders are added to make the real-time calculations simple. The arm is naturally compliant (because of the springs) and this gives the arm the ability to exert controllable grasp forces and counteract disturbances.

The spring system for one limb is shown in Figure 2. A compression and an extension spring are mounted coaxially to allow forces to be transmitted in both directions. Linear steel slides are added to support the springs and keep their motion straight.
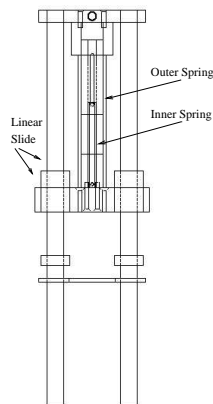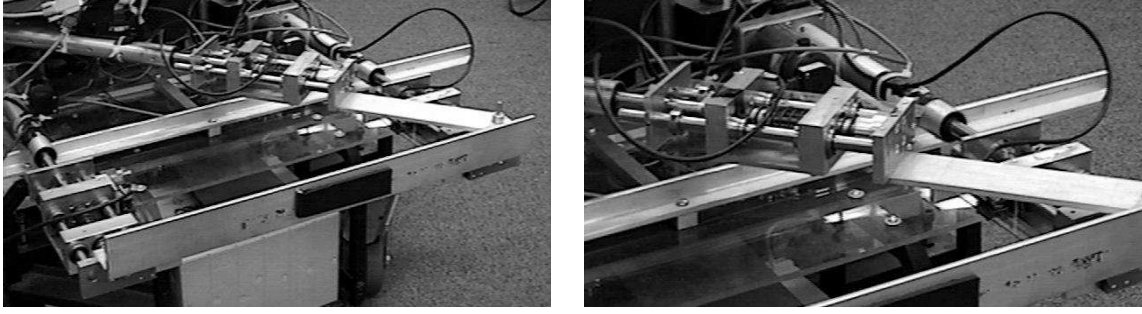

Figure 2.   The spring system for one limb.

3   Copyright © 2000 by ASME

Figure 3. The three degree-of-freedom, in-parallel, actively controlled arm applies a force in the X and Y directions as well as a moment in the Z direction. Each limb has a spring attached in series to a linear actuator driven by a DC motor attached to a ball screw transmission.

2.2 Kinematics

It is possible to determine the position of the end effector from the three link lengths. A more general study describing the kinematics of multiple chained truss mechanisms is described in (Padmanabhan et al., 1992). First, inside angles must be determined. See Figure 4.
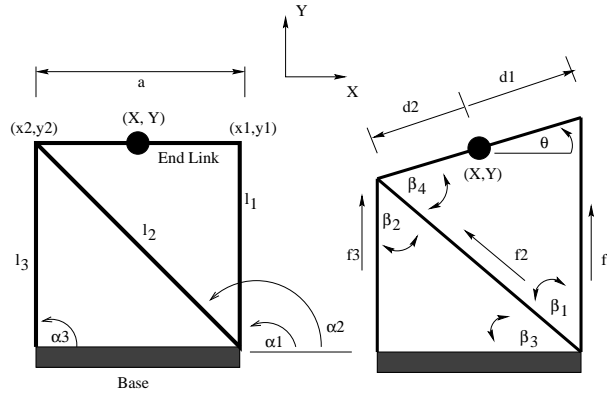

Figure 4. A schematic of the parallel manipulator.

$$\beta_1 = \arccos\frac{l_1^2 + l_2^2 - a^2}{2l_1l_2}, \quad \beta_2 = \arccos\frac{l_2^2 + l_3^2 - a^2}{2l_2l_3} \tag{1}$$

$$\beta_3 = \arccos\frac{l_2^2 + a^2 - l_3^2}{2l_2a}, \quad \beta_4 = \arccos\frac{l_2^2 + a^2 - l_1^2}{2l_2a} \tag{2}$$

There are four cases for the mechanism because the angle α_1 can lie in all four quadrants. For now, it can be assumed that all of the angles are positive, but the assumption is not needed in the actual mechanism since the angles are automatically measured to ease calculations. Also, the real mechanism cannot fold in on itself.

4

The coordinates of the moving pivots on the end effector (x_i, y_i) can be determined (assuming β_i's are positive).

$$x_1 = l_1 \cos\alpha_1 + a = l_1 \cos(\pi - \beta_1 - \beta_3) + a, \quad y_1 = l_1 \sin\alpha_1 = l_1 \sin(\pi - \beta_1 - \beta_3) \tag{3}$$

$$x_2 = l_3 \cos\alpha_3 = l_3 \cos(\pi - \beta_2 - \beta_3), \quad\quad y_2 = l_3 \sin\alpha_3 = l_3 \sin(\pi - \beta_2 - \beta_3) \tag{4}$$

Lastly, the position of the end effector can be determined.

$$x = \frac{(x_1 + x_2)}{2}, \quad y = \frac{(y_1 + y_2)}{2}, \quad \theta = \arctan\left(\frac{(y_1 - y_2)}{(x_1 - x_2)}\right) \tag{5}$$

2.3 Optimal Design

Two candidate designs for the manipulator geometry are shown in Figure 5. The one on the right has a Jacobian matrix with a larger determinant. This has the desirable effect of improving the transmission characteristics of the linkage. However, this design is not very compact. Thus, the geometry on the left proves to be a good compromise. Details on optimizing an in-parallel planar platform are described by Lee et al. (1996). The optimal solution is a moving equilateral triangle which has a determinant 2.12 times as large, but the mechanism is 1.7 times as large as the current one that is built.
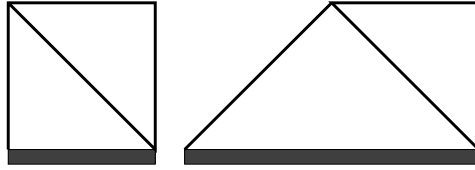

Figure 5. Candidate designs. The design on the right possesses optimal transmission characteristics but is too bulky while the design on the left is the compromise design.

In the initial design stage, an arm with a straight end effector is considered because this type of mechanism will allow easy mating with different objects. The two competing designs are shown in Figure 5. For completeness, a study of parallel planar mechanisms is given next.

In the general case, the determinant of the Jacobian matrix for the parallel mechanism gives a measure of the transmission characteristics. Instead of using a geometric viewpoint, an easier method is to treat the design as an optimization problem, maximizing the determinant. Using the method of boundedness checking, the optimal problem can be simplified by verifying the model. Given the parallel mechanism in Figure 6, the determinant can be easily found. The limbs are shown by heavy black lines and their angles from the horizontal line are given by α_1, α_2, and α_3. The radial length from the origin to each limb is given by a_1, a_2, and a_3 and the angle that each radius makes with the horizontal line is given by θ_1, θ_2, and θ_3 respectively.

$$B = \begin{pmatrix} \cos\alpha_1 & \cos\alpha_2 & \cos\alpha_3 \\ \sin\alpha_1 & \sin\alpha_2 & \sin\alpha_3 \\ a_1 \sin(\alpha_1 - \theta_1) & a_2 \sin(\alpha_2 - \theta_2) & a_3 \sin(\alpha_3 - \theta_3) \end{pmatrix} \tag{6}$$

$$|B| = a_1 \sin(\alpha_2 - \alpha_1)\sin(\alpha_3 - \theta_3) + a_2 \sin(\alpha_3 - \alpha_2)\sin(\alpha_1 - \theta_1) + a_3 \sin(\alpha_1 - \alpha_3)\sin(\alpha_2 - \theta_2) \tag{7}$$
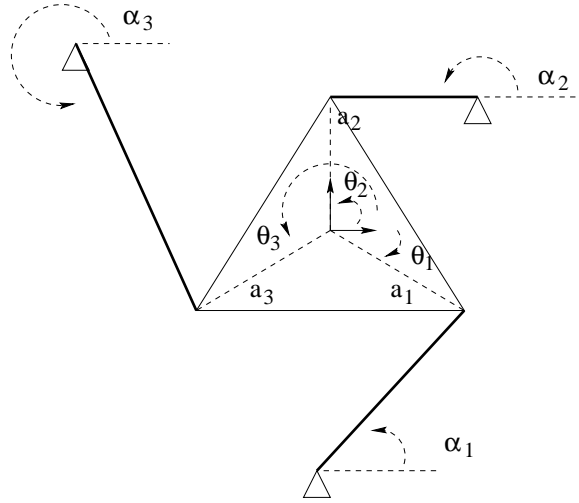
5

Figure 6. General planar parallel mechanism.

The optimal problem is to maximize the determinant with nine variables. This problem is very difficult, but the problem can be reduced to maximizing the determinant with only six variables. The angles, θ_1, θ_2, and θ_3, cannot be chosen arbitrarily. The angles must be chosen to insure that each respective term equals 1 depending on the sign of the first function in each term.

$$(\alpha_3 - \theta_3) = sign(\sin(\alpha_2 - \alpha_1))\frac{\pi}{2} \tag{8}$$

$$(\alpha_1 - \theta_1) = sign(\sin(\alpha_3 - \alpha_2))\frac{\pi}{2} \tag{9}$$

$$(\alpha_2 - \theta_2) = sign(\sin(\alpha_1 - \alpha_3))\frac{\pi}{2} \tag{10}$$

The problem reduces to maximizing a simpler determinant.

$$det = a_1 \sin(\alpha_2 - \alpha_1) + a_2 \sin(\alpha_3 - \alpha_2) + a_3 \sin(\alpha_1 - \alpha_3) \tag{11}$$

Using an optimization program, the problem can be solved once values are assigned for the lengths, a_1, a_2, and a_3. If the lengths are all equal, then the problem reduces to the same answer that Lee et al. (1996) found. They assume that the lengths all equal one, but if all of the lengths equal 2, the same answer will be found but obviously the determinant will be twice as large as the first one. In the simple case of equal lengths, the difference between the angles, α_1, α_2, and α_3 must equal 120 degrees in order to maximize the original determinant. If the lengths are different sizes, then different mechanisms will be determined. This optimal mechanism with equal lengths is shown in Figure 6.

Our mechanism was designed based on two assumptions. First, it is assumed that the lengths, a_1, a_2, and a_3, are all equal, and $\theta_1 = 0$, $\theta_2 = 180$, and $\theta_3 = 180$. Our design required a flat end effector; thus the values for θ_i are determined by the design specifications. With these values, the simplified determinant can be found and a different function is optimized.

$$det = \sin(\alpha_1 - \alpha_2)\sin(\alpha_3) + \sin(\alpha_3 - \alpha_2)\sin(\alpha_1) + \sin(\alpha_3 - \alpha_1)\sin(\alpha_2) \tag{12}$$
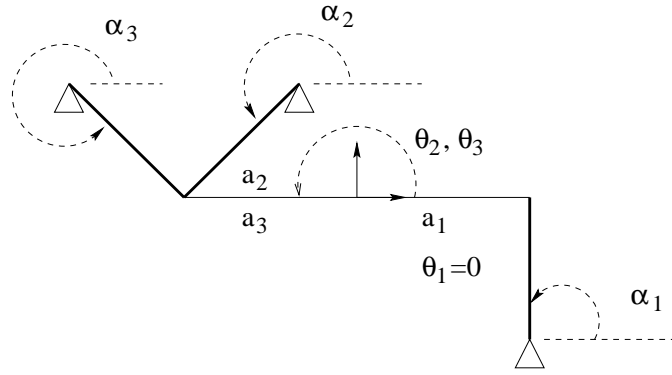
6

Figure 7. Optimal planar parallel mechanism with constraints on the internal angles θ_1, θ_2, and θ_3.

One solution to maximize the new determinant can be found. See Figure 7.

$$\alpha_1 = 90, \theta_1 = 0 \tag{13}$$

$$\alpha_2 = 225, \theta_2 = 180 \tag{14}$$

$$\alpha_3 = 315, \theta_3 = 180 \tag{15}$$

Note as stated before, this solution has a smaller determinant than the optimal solution with all angles, α, being 120 degrees apart, but this solution is more compact. All of the solutions given assume equal lengths, reducing the complexity of the problem. This optimal mechanism for straight end effectors in Figure 7 is the same mechanism shown on the right in Figure 5.

2.4 Singularities

The singularities occur when the determinant equals zero or when it is undefined. For our design the determinant equals:

$$det = \frac{a}{2}\left(\sin\left(\alpha_2 - \alpha_1\right)\sin\left(\theta - \alpha_3\right)\right) + \frac{a}{2}\left(\sin\left(\alpha_3 - \alpha_2\right)\sin\left(\alpha_1 - \theta\right)\right) + \frac{a}{2}\left(\sin\left(\alpha_1 - \alpha_3\right)\sin\left(\theta - \alpha_2\right)\right) \tag{16}$$

which follows from

$$\theta_1 = \theta, \quad \theta_2 = \pi + \theta, \quad \theta_3 = \pi + \theta \tag{17}$$

and

$$a_1 = \frac{a}{2}, \quad a_2 = \frac{a}{2}, \quad a_3 = \frac{a}{2}. \tag{18}$$

The determinant is undefined when:

$$a = 0 \quad \text{or} \tag{19}$$

$$\alpha_1 = \alpha_2 = \alpha_3 \quad \text{or} \tag{20}$$

$$\alpha_1 = \theta, \quad \alpha_1 = \theta + \pi \quad \text{or} \tag{21}$$

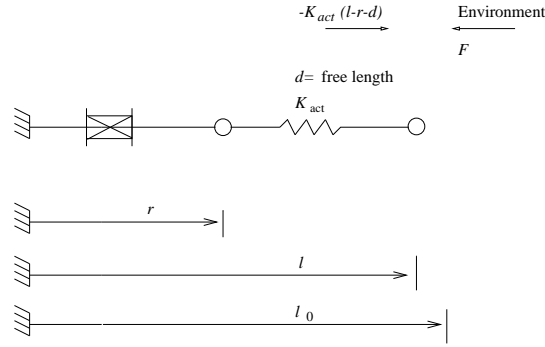$$\alpha_2 = \alpha_3, \quad \alpha_2 = \alpha_3 + \pi. \tag{22}$$
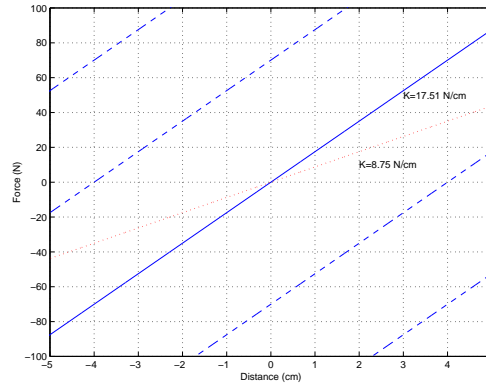
7

Figure 8.   Model of one link.

Figure 9.   Force deflection curves for the adjustable spring system.

Singularities do not occur because the end effector has a finite length and the limbs cannot reach the configurations that cause poor performance.

3   Arm Control

The previous section described the kinematics and the design of a novel manipulator for mobile platforms. A key aspect of this arm is the use of springs that allow the control of the arm to use simple position control schemes. In this section, stiffness control for one limb and the entire arm are presented with experimental results. The stiffness of the contact represented by a planar stiffness matrix can be prescribed by the user allowing the system's grasp to be adjustable.

3.1   Stiffness Control for One Link

The control of a single actuator-spring system is best explained with the help of Figures 8-9. One end of the spring assembly is driven by the linear actuator while the other end is attached to the end effector. The actuator controls the extension r while the environment constrains the extension l. The force balance of the link is given by

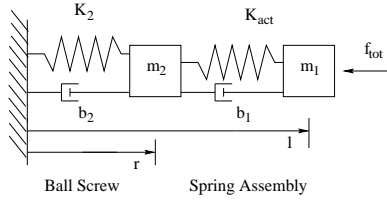$$F = -K_{act}(l - r - d) \tag{23}$$

8

Figure 10.   Model of one link.

where d describes the free length of the spring and F describes the reaction force from the environment. The length, $(l-r-d)$, describes the deflection of the spring. If we desire a different spring behavior for the *link* given by

$$F = -K_{des}(l - l_o) + f_{des} \tag{24}$$

about an operating point (f_{des}, l_o), the desired actuator position is

$$r_{des} = \frac{f_{des} + K_{des}l_o + l(K_{act} - K_{des}) - K_{act}d}{K_{act}}. \tag{25}$$

The values for the desired stiffness K_{des}, the preload force f_{des}, and the home position of the link l_o are chosen by the designer. Thus a simple position control scheme achieves a desired stiffness of a one link system.

The natural mechanical stiffness of the spring, K_{act}, is shown by the solid line in Figure 9. The dashed lines show other possible force-deflection curves that are obtained by simply shifting the equilibrium position of the spring. More importantly, the extension r can be controlled to obtain any force-deflection curve with a slope smaller than K_{act}. The dotted line in the figure shows a new possible force-deflection curve that can be obtained via a suitable position control scheme given by Equation (25).

3.1.1   Analysis of Stiffness Control for One Link   The ability of one link to maintain a desired stiffness can also be analyzed. See Figure 10. If f_{des} and l_o are both taken to be zero, then the analysis simplifies and a transfer function for the stiffness of the link can be computed.

The stiffness of the link can be computed in terms of the spring force that is generated or in terms of the actual total force. The total force includes the inertia term which hampers the performance of the system only at high frequencies.

The movement of the mass, m_1, is measured by the length, l, while q measures the movement of the mass, m_2. The length, q, simplifies the equations and is defined below.

$$q = r + d \tag{26}$$

$$q_{des} = r_{des} + d \tag{27}$$

The dynamics of the *spring assembly* are found by summing the forces.

$$-K_{act}(l - q) - f_{tot} = m_1 \ddot{l} + b_1(\dot{l} - \dot{q}) \tag{28}$$

The simple position control law can be found assuming f_{des} and l_o both equal zero.

$$q_{des} = l - l\frac{K_{des}}{K_{act}} \tag{29}$$

9   Copyright © 2000 by ASME
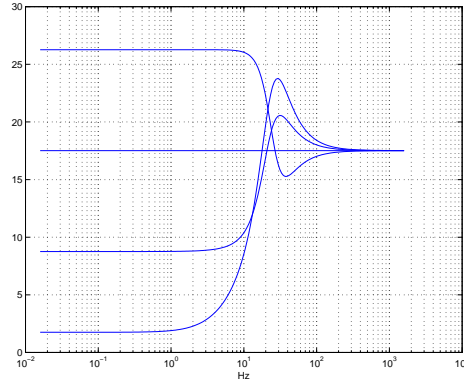
Figure 11. Different transfer functions for the stiffness control of one link as K_{des} is varied from 1.75 to 26.27 N/cm and K_{act} equals 17.51 N/cm. The transfer function compares the spring force to the link defection, $\frac{f_{spring}(s)}{l(s)}$.

The dynamics of the ball screw assembly are modeled using a second order system. The controller, motor inertia, and torque constant are all lumped into the second order system. The transfer function, $\frac{q(s)}{q_{des}(s)}$, describes the ability of the motor to move the mass, m_2. Because of the addition of a proportional and derivative controller, the mass system is described with a spring constant as well as a damping constant.

$$\frac{q(s)}{q_{des}(s)} = \frac{K_2}{m_2 s^2 + b_2 s + K_2}$$

The transfer function is determined experimentally and the bandwidth of the servo system is 24 Hz.

Symbol	Definition	Value
m_1	Mass at the end of the limb	0.0063 kg $\frac{m}{cm}$
b_1	Damping in the linear bearings	0.0933 N $\frac{s}{cm}$ +/- 0.0009
K_{act}	Actual spring stiffness	17.51 $\frac{N}{cm}$
m_2	Mass of the ball screw and spring assembly	0.0181 kg $\frac{m}{cm}$
b_2	Damping of the ball screw assembly (experimentally determined)	2.98 N $\frac{s}{cm}$
K_2	Spring constant of the ball screw assembly (experimentally determined)	412.23 $\frac{N}{cm}$

The transfer function for the stiffness of one link in terms of the spring force is given.

$$\frac{f_{spring}(s)}{l(s)} = \frac{-K_{act}m_2 s^2 - K_{act}b_2 s - K_2 K_{des}}{m_2 s^2 + b_2 s + K_2} \tag{30}$$

As K_{des} is varied different curves are generated. See Figure 11. Good results for stiffness values between 8.756 and 26.27 N/cm can be seen in the diagram. At very high frequencies, the motor will no longer move and the stiffness value of the link will converge to the nominal value of 17.51 N/cm.

If the total force is compared to the link deflection, then the performance of the system degrades. See Figure 12. In all cases with different desired stiffness values, the inertia term deflects the curve at frequencies above 2 Hz. The transfer function comparing the total
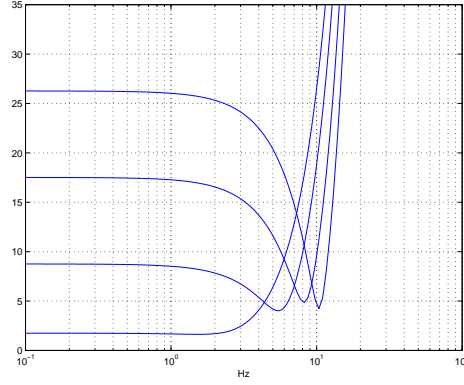
Figure 12. Different transfer functions for the stiffness control of one link as K_{des} is varied from 1.75 to 26.27 N/cm and K_{act} equals 17.51 N/cm. The transfer function compares the total force to the link defection, $\frac{f_{tot}(s)}{l(s)}$. At high frequencies, the mass m_1 dominates the response.

force to the link defection is given.

$$\frac{f_{tot}(s)}{l(s)} = \frac{-m_1 m_2 s^4 - (m_1 b_2 + m_2 b_1)s^3 - (K_2 m_1 + b_1 b_2 + K_{act} m_2)s^2}{m_2 s^2 + b_2 s + K_2} + \frac{-(K_{act} b_2 + \frac{b_1 K_2 K_{des}}{K_{act}})s - K_{des} K_2}{m_2 s^2 + b_2 s + K_2}$$ (31)

At high frequencies the curve is determined by the inertia of the system.

$$\frac{f_{tot}(s)}{l(s)} = -m_1 s^2$$ (32)

The inertia term is not experimentally canceled using a controller because acceleration sensors are very noisy and more importantly the motor will not be able adjust its position quickly enough. Note if the input is bounded then the output will be bounded as well.

3.2 Stiffness Control for the Arm

In the three degree-of-freedom system, the Cartesian stiffness can be controlled to achieve a desired stiffness. Let the Cartesian position be given by the coordinates of the reference point on the end effector (X, Y), and let θ be the orientation of the end effector as shown in Figure 4.

If the desired Cartesian stiffness is given by

$$\begin{pmatrix} \Delta F_x \\ \Delta F_y \\ \Delta M \end{pmatrix} = \begin{pmatrix} K_{xx} & K_{xy} & K_{x\theta} \\ K_{yx} & K_{yy} & K_{y\theta} \\ K_{\theta x} & K_{\theta y} & K_{\theta\theta} \end{pmatrix} \begin{pmatrix} \Delta X \\ \Delta Y \\ \Delta\theta \end{pmatrix}$$ (33)

the desired joint stiffness matrix for the joints is:

$$k = B^{-1} K B^{-T} = \begin{pmatrix} k_{11} & k_{12} & k_{13} \\ k_{21} & k_{22} & k_{23} \\ k_{31} & k_{32} & k_{33} \end{pmatrix}$$ (34)

11

where

$$B = \begin{pmatrix} \cos\alpha_1 & \cos\alpha_2 & \cos\alpha_3 \\ \sin\alpha_1 & \sin\alpha_2 & \sin\alpha_3 \\ C_1 & C_2 & C_3 \end{pmatrix}. \tag{35}$$

The vectors and symbols are defined below.

$$C_1 = 1/2(x_1 - x_2)\sin\alpha_1 - 1/2(y_1 - y_2)\cos\alpha_1 \tag{36}$$

$$C_2 = 1/2(x_2 - x_1)\sin\alpha_2 - 1/2(y_2 - y_1)\cos\alpha_2 \tag{37}$$

$$C_3 = 1/2(x_2 - x_1)\sin\alpha_3 - 1/2(y_2 - y_1)\cos\alpha_3 \tag{38}$$

$$x_1 = l_1\cos\alpha_1 + a, \quad y_1 = l_1\sin\alpha_1 \tag{39}$$

$$x_2 = l_3\cos\alpha_3, \quad y_2 = l_3\sin\alpha_3 \tag{40}$$

The matrix B and the Jacobian matrix J are related because of the duality principle. The matrix B is defined for simplicity since the Jacobian matrix is very difficult to calculate for parallel manipulators. The matrix, B, relates the joint forces to the Cartesian Forces.

$$\begin{pmatrix} F_x \\ F_y \\ M \end{pmatrix} = B \begin{pmatrix} f_1 \\ f_2 \\ f_3 \end{pmatrix} \tag{41}$$

The Jacobian matrix, J, relates the joint velocities to the end effector velocities and is used to transform the desired Cartesian stiffness matrix to the joint stiffness matrix.

$$\begin{pmatrix} v_x \\ v_y \\ \omega \end{pmatrix} = J \begin{pmatrix} \dot{l}_1 \\ \dot{l}_2 \\ \dot{l}_3 \end{pmatrix} \tag{42}$$

$$k = J^T K J \tag{43}$$

From the principle of virtual work (Asada and Slotine, 1986), we can easily show that

$$B = J^{-T} \tag{44}$$

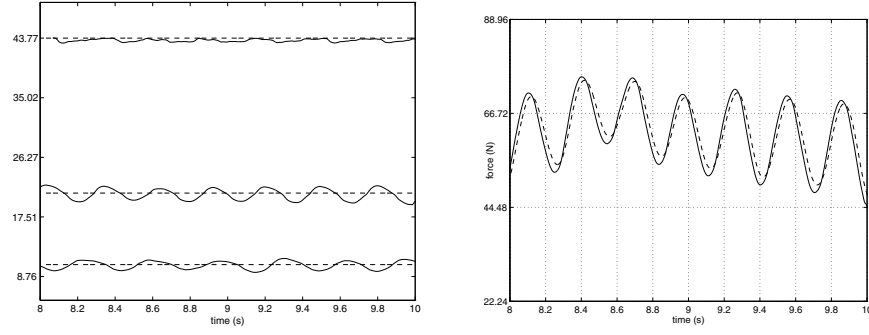and Equation (34) can be derived from Equations (43) and (44).

Figure 13. Stiffness in the normal direction, desired (dashed) and actual. The normal force when $K_{yy} = 21.04$ N/cm is shown on the right.

To achieve the desired Cartesian stiffness, the individual links must be controlled in real time to maintain the desired joint stiffness k. Equations (23,24,25) can be written in vector form as shown below:

$$\vec{F} = -K_{act}(\vec{l} - \vec{r} - \vec{d}) \tag{45}$$

$$\vec{F} - \vec{f}_{des} = -k(\vec{l} - \vec{l}_o) \tag{46}$$

$$\vec{r}_{des} = K_{act}^{-1}(\vec{f}_{des} + (K_{act} - k)\vec{l} + k\vec{l}_o - K_{act}\vec{d}) \tag{47}$$

$\vec{F}$ is a vector of joint forces and $\vec{r}_{des}$ is a vector of desired joint positions to send to the embedded motor controllers.

3.3 Arm Experiments Using Stiffness Control

The following table gives the actual stiffness parameters of the mechanism in the home position with the motors turned off.

Stiffness Coefficient	Value
K_{xx}	8.756 N/cm
K_{yy}	43.78 N/cm
$K_{\theta\theta}$	28240 Ncm/rad
$K_{xy} = K_{yx}$	-8.756 N/cm
$K_{x\theta} = K_{\theta x}$	-222.4 N/rad
$K_{y\theta} = K_{\theta y}$	1112 N/rad

The ability to control the Cartesian stiffness is demonstrated in Figure 13. The stiffness in the normal direction can be varied from roughly $K_{yy} = 10.51$ to 43.78 N/cm. The ability of the arm to maintain a desired stiffness is shown for three different values in Figure 13. As the desired stiffness decreases, the actuators must move through larger distances which in turn reduces the frequency response. In these trials, the desired stiffness is a constant (10.51, 21.01, and 43.78 N/cm respectively), but the actual stiffness varies around the nominal desired value. A representative force history shown in Figure 13(right) illustrates that the arm closely follows the desired force.

In the tangential direction, the stiffness, K_{xx}, can be varied from 5.25 to 10.51 N/cm. See the results for three different trials in Figure 14. These plots look much better because link 2 contributes the majority of the force in the tangential direction and there is less coupling than in the normal direction. The actual force follows the desired force very well. See Figure 14(right).
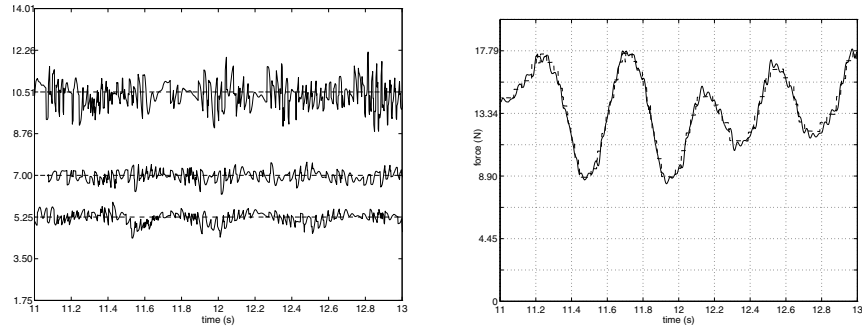
13

Figure 14. Stiffness in the tangential direction, desired (dashed) and actual. The tangential force when $K_{xx} = 7.00$ N/cm is shown on the right.
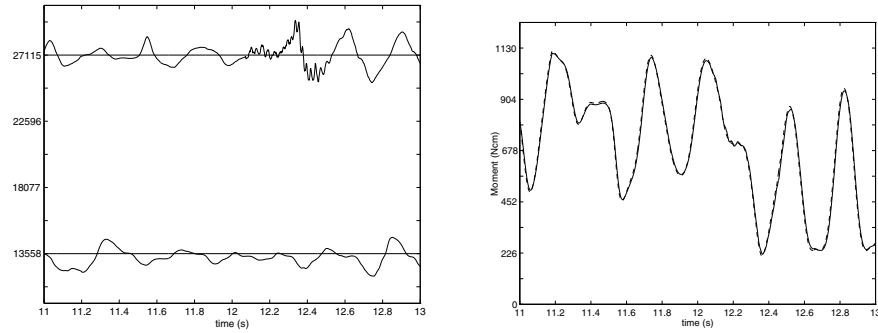

Figure 15. Angular stiffness, desired (dashed) and actual. The moment when $K_{\theta\theta} = 27110$ Ncm/rad is shown on the right.

In the angular direction, the stiffness can be varied from $K_{\theta\theta} = 13560$ to 27110 Ncm/rad. Again, the moment closely matches the desired moment. See Figure 15(right). The actual angular stiffness varies because as the desired moment nears zero, any small errors are magnified.

Other experiments were also conducted to determine the performance of the arm. Three sample experiments were performed to determine the desired Cartesian stiffness matrix versus the actual Cartesian stiffness matrix. In these experiments, the controller maintains a force law based on the desired Cartesian stiffness matrix as the arm is moved. While the arm is moved in three directions, the link deflections as well as the link forces are stored in a file. The link forces as well as link deflections are converted to Cartesian forces and Cartesian deflections, and compared. Using a simple least squares fit with hundreds of data points, the six parameters of the actual Cartesian stiffness matrix are estimated.

In the first example, the desired Cartesian stiffness matrix is diagonal which is a typical matrix used in the robot experiments. The actual stiffness matrix is close to diagonal. The actual stiffness for $K_{\theta\theta}$ is larger than the desired value of 2260 Ncm/rad but is still much smaller than the nominal value of 28244.8 Ncm/rad.

In the second example, the desired Cartesian stiffness matrix is no longer diagonal and emphasizes that the system can control all six values of the stiffness matrix. In this example, the larger desired value for $K_{\theta\theta}$ matches the actual value much better. Again, the value for $K_{x\theta}$ is smaller than the desired value of 22.24, but is much different than the nominal value of -222.4 N/rad.

In the third example, the sign of the off diagonal terms is changed to better match the nominal values of the system. In this example, the actual values match the desired values very well.

In all three cases, it is noted that the links must move a finite distance unless the desired values match the nominal values of the arm. If the desired stiffness is much smaller than the actual stiffness, the arm must move further and the errors will be larger.

14

Desired Cartesian
Stiffness Matrix

$$\begin{pmatrix} 1.75 & 0 & 0 \\ 0 & 3.50 & 0 \\ 0 & 0 & 2260 \end{pmatrix}$$

$$\begin{pmatrix} 5.25 & 1.75 & 22.2 \\ 1.75 & 17.51 & 111 \\ 22.2 & 111 & 11300 \end{pmatrix}$$

$$\begin{pmatrix} 5.25 & -1.75 & -22.2 \\ -1.75 & 17.51 & 111 \\ -22.2 & 111 & 11300 \end{pmatrix}$$

Actual Cartesian Stiffness
Matrix Obtained by Averaging

$$\begin{pmatrix} 1.72 & 0 & 0.67 \\ 0 & 3.45 & -1.42 \\ 0.67 & -1.42 & 2570 \end{pmatrix}$$

$$\begin{pmatrix} 4.938 & 1.65 & 13.0 \\ 1.65 & 17.37 & 110 \\ 13.0 & 110 & 11400 \end{pmatrix}$$

$$\begin{pmatrix} 4.938 & -1.68 & -22.5 \\ -1.68 & 17.41 & 111 \\ -22.5 & 111 & 11300 \end{pmatrix}$$

Table 1.   Typical experiments controlling the stiffness of the arm.

4   Conclusions

The new actuator, a ball screw with a spring in series, can be used to control the force or stiffness of a limb with simple position control laws. Three identical limbs can be used in a parallel mechanism to allow the forces and moment in the plane to be controlled. If the forces in each limb can be controlled then the stiffness of the limb or mechanism can be controlled as well.

The force control bandwidth for one limb is 24 Hz if the end-effector is fixed. The limitations of the system are caused by the bandwidth of the motor control system and ignoring the inertia of the end effector. The inertia is ignored because it depends on the payload which can vanish. One way of estimating the inertia is via an accelerometer, but it is very noisy and the motor control bandwidth is low as well.

The desired planar stiffness matrix for the mechanism is adjustable and can be varied over a wide range; the six stiffness coefficients can all be adjusted. The tangential stiffness was varied between 1.75 and 14.0 N/cm and the normal stiffness from 3.5 to 43.78 N/cm. The angular stiffness was varied between 2260 and 27115 Ncm.

The control system is very simple and uses DC motors with embedded motor controllers. The position setpoints are sent to the motor controllers and simple linear controllers are used. The system is robust to positioning errors and disturbances because it is inherently passive and the equilibrium position of the springs is only adjusted. During the transition between not contacting the object and contacting the object, the system is passive and no instabilities occur. Complicated current or torque control is not used. The backlash and gearing of the motor are ignored because the force is measured by the deflection of the spring at the end of the actuator system. The mechanism can accommodate platform positioning errors by extending or retracting the limbs and can control the grasp forces applied to the object.

REFERENCES

Asada, H. and Slotine, J.-J. E., 1986, *Robot Analysis and Control*, John Wiley and Sons.

Colgate, J. E. and Hogan, N., 1988, "Robust Control of Dynamically Interacting Systems," *International Journal of Control*, Vol. 48, No. 1, pp. 65–88.

Eppinger, S. and Seering, W., 1986, "On Dynamic Models of Robot Force Control," in: *Proceedings of the IEEE International Conference on Robotics and Automation*, pp. 29–34.

Howell, L., Midha, A., and Murphy, M. D., 1994, "Dimensional Synthesis of Compliant Constant-Force Slider Mechanisms," in: *Machine Elements and Machine Dynamics, 23rd Biennial ASME Mechanisms Conference, DE-71*, Minneapolis.

Kazerooni, H., Houpt, P. K., and Sheridan, T. B., 1986a, "Robust Compliant Motion for Manipulators, Part 2: Design Method," *IEEE Journal of Robotics and Automation*, Vol. RA-2, No. 2, pp. 93–105.

Kazerooni, H., Sheridan, T. B., and Houpt, P. K., 1986b, "Robust Compliant Motion for Manipulators, Part 1: The Fundamental Concepts of Compliant Motion," *IEEE Journal of Robotics and Automation*, Vol. RA-2, No. 2, pp. 83–92.

Kolacinski, R. and Quinn, R., 1998, "Design and Mechanics of an Antagonistic Biomimetic Actuator System," in: *Proceedings of 1998 International Conference on Robotics and Automation*, Belgium.

Lee, J., Duffy, J., and Keler, M., 1996, "The Optimum Quality Index for the Stability of In-Parallel Planar Platform Devices," in: *Proceedings of the 1996 ASME Design Engineering Technical Conferences and Computers in Engineering Conference*, Irvine, California.

Mason, M. T., 1981, "Compliance and Force Control for Computer Controlled Manipulators," *Transactions on Systems, Man, and Cybernetics*, Vol. SMC-11, No. 6, pp. 418–432.

Morrell, J. and Salisbury, J., 1995, "Parallel Coupled Actuators for High Performance Force Control: A Micro-Macro Concept," in: *Proceedings of the 1995 IEEE/RSJ International Conference on Intelligent Robots and Systems*.

Padmanabhan, B., Arun, V., and Reinholtz, C., 1992, "Closed-Form Inverse Kinematic Analysis of Variable-Geometry Truss Manipulators," *Journal of Mechanical Design*, Vol. 114.

Paul, R. and Shimano, B., 1976, "Compliance Control," in: *In Proceedings of the JACC*.

Pfreundschuh, G., Sugar, T., and Kumar, V., 1994, "Design and control of a three-degrees-of-freedom, in-parallel, actuated manipulator," *Journal of Robotic Systems*, Vol. 11, No. 2.

Pratt, G. and Williamson, M., 1995, "Series Elastic Actuators," in: *Proceedings of the 1995 IEEE/RSJ International Conference on Intelligent Robots and Systems*.

Salisbury, J. K., 1980, "Active stiffness control of a manipulator in Cartesian coordinates," in: *19th IEEE Conf. on Decision and Control*.

Sugano, S., Tsuto, S., and Kato, I., 1992, "Force Control of the Robot Finger Joint Equipped with Mechanical Compliance Adjuster," in: *Proceedings of the 1992 IEEE/RSJ International Conference on Intelligent Robots and Systems*, Raleigh, NC.

Tasch, A. D. U., 1996, "A Two-DOF Manipulator with Adjustable Compliance Capabilities and Comparison with the Human Finger," *Journal of Robotic Systems*, Vol. 13, No. 1.

Volpe, R. and Khosla, P. K., 1992, "An Experimental Evaluation and Comparison of Explicit Force Control Strategies for Robotic Manipulators," in: *Proceedings of 1992 International Conference on Robotics and Automation*.

Whitney, D. E., 1985, "Historical Perspective and State of the Art in Robot Force Control," in: *Proceedings of 1985 International Conference on Robotics and Automation*.

Xu, Y. and Paul, R., 1988, "On Position Compensation and Force Control Stability of a Robot with a Compliant Wrist," in: *Proceedings of 1988 International Conference on Robotics and Automation*.